https://doi.org/10.5194/egusphere-2022-1450
Preprint. Discussion started: 23 December 2022

A robust framework for comparing Lagrangian and gridded Eulerian velocity fields: an example application to surface drifters and altimetry-derived surface currents

Arthur Coquereau[1, 2] and Nicholas P. Foukal[2]

[1]Laboratoire d'Océanographie Physique et Spatiale, Univ. Brest CNRS IRD Ifremer, Brest, France
[2]Woods Hole Oceanographic Institution, Woods Hole, MA 02543, USA

Correspondence: Arthur Coquereau (arthur.coquereau@univ-brest.fr)

Abstract. A novel framework for comparing Lagrangian and gridded Eulerian velocity fields is proposed. The method involves three steps that individually leverage the strengths of each reference frame to provide robust intercomparisons, while also allowing the user to adapt the individual steps to the process of interest. The utility of the methodology is then demonstrated by applying it to a comparison between a set of 34 Lagrangian surface drifters deployed on the continental shelf around the southern tip of Greenland and Eulerian altimetry-derived surface currents with and without Ekman velocities. We conclude that the methodology sufficiently addresses differences between the reference frames and accurately identifies errors when they exist. This result enables us to conclude that the altimetry-derived surface currents accurately resolve the important components of the shelf circulation around the southern tip of Greenland and can be used to track pathways of fresh water around Greenland.

1 Introduction

There are two reference frames from which a flow field can be measured: (1) the Eulerian reference frame in which velocities are measured from a fixed geographic location, and (2) the Lagrangian reference frame in which velocities are measured along a fluid trajectory. These two perspectives serve as complementary views on the same underlying physical system; thus, their results should converge if the system is fully constrained. However, observations of geophysical flow fields such as of the atmosphere and ocean are under sampled and contain uncertainty that is difficult to quantify. It is often useful to compare data from these two reference frames so that their data streams can be combined, and their errors assessed against one another.

Despite this utility, directly comparing Eulerian and Lagrangian data is difficult because the reference frames provide fundamentally different information about the flow field. Eulerian data inform how the flow field evolves through time, while Lagrangian data provide information on the origin, pathways and fate of fluid particles. The spatial scales also typically vary between these two reference frames. While Eulerian data can come from point measurements or data mapped onto a regular grid that typically cover larger spatial scales, Lagrangian data only come from point measurements, typically on smaller scales. Comparing point measurements from Eulerian and Lagrangian reference frames is not useful in most applications – these two data streams are only directly comparable when they physically intersect, and when they do, it is straightforward to compare them. Thus, we do not discuss this comparison any further. In contrast, the need to compare gridded Eulerian data

https://doi.org/10.5194/egusphere-2022-1450
Preprint. Discussion started: 23 December 2022

with Lagrangian data arises quite often in oceanography. The proliferation of gridded satellite and reanalysis products, as well as numerical model output has produced a large number of gridded Eulerian data sets (e.g., Haine et al., 2021). These data sets are often compared to surface drifters from the Global Drifter Program (GDP; Lumpkin and Johnson, 2013) and profiling floats from the Argo network (Johnson et al., 2022) to yield a velocity field that utilizes the accuracy of the in situ Lagrangian data with the spatial perspective of the gridded Eulerian data.

Though the need for a robust framework for comparing gridded Eulerian and Lagrangian velocities exists, there is not yet a well-accepted, published methodology for these comparisons. Previous work on this topic typically converts one of the data sets into the other reference frame, then applies standard statistical methods such as correlation or variance metrics (Liu and Weisberg, 2011; Liu et al., 2014; Rio et al., 2011; Pujol et al., 2016; Rio and Santoleri, 2018; Mulet et al., 2021). This can be done by either gridding Lagrangian velocities onto a Eulerian grid or simulating Lagrangian trajectories through a Eulerian velocity field. While both methods yield data sets that can be directly compared, the process of transforming the data between reference frames inevitably degrades the converted data by interpolating or extrapolating when/where data is not available. If this comparison is only done in one direction, this process likely biases the results toward one reference frame. Thus, to robustly compare Eulerian and Lagrangian data, this conversion must proceed in both directions.

In this work, we propose a framework that involves three analysis steps to directly compare Eulerian and Lagrangian velocity fields. The framework addresses three questions that leverage the relative strengths of each perspective:

- Question #1: How well do the gridded Eulerian velocities resolve the velocities directly observed by the Lagrangian platform? Analysis: Directly compare the velocity fields at collocated and contemporaneous points.
- Question #2: How well do the Lagrangian data recover the spatial structure of the gridded Eulerian data? Analysis: Map the Lagrangian velocities onto a Eulerian grid.
- Question #3: How well do the Eulerian data capture the origins, pathways, fate, and connectivity of water masses? Analysis: Simulate Lagrangian trajectories in the Eulerian flow fields.

The first step directly compares the two data sets without any transformation between reference frames, while the second two steps convert one data set into the other's reference frame. All three steps utilize the strengths of the data sets: the accuracy of the Lagrangian data (#1), the spatial perspective of the Eulerian data (#2), and the origins, pathways, fate, and connectivity of the Lagrangian data (#3). The novelty in this method comes from the combination of these three steps, as each have been used individually in various other works.

The rest of this paper is organized in a manner to introduce this three-step methodology to oceanography. In the following section, we describe the rationale behind this methodology and describe its application in general terms with some schematic illustrations. In section three, we describe an application of the methodology to a pilot study comparing altimetry-derived surface currents (ADSC) and velocities from surface drifters near the southern tip of Greenland. Finally, conclusions will be presented in the fourth section.

https://doi.org/10.5194/egusphere-2022-1450
Preprint. Discussion started: 23 December 2022

2 Comparison framework

2.1 Point-wise comparison between gridded Eulerian and Lagrangian velocity fields

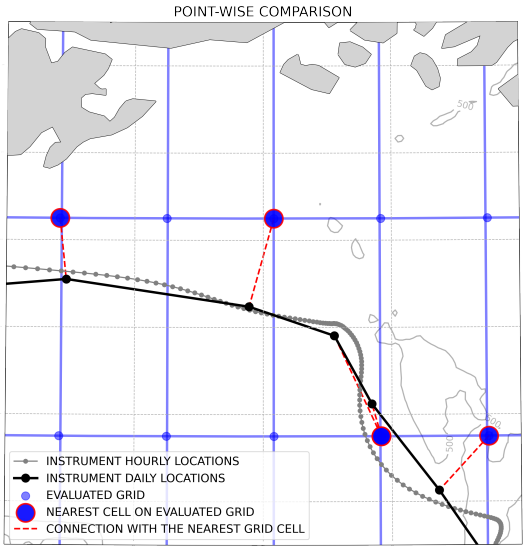

Figure 1. Representation of the point-wise comparison. The hourly Lagrangian trajectory (gray) is averaged to daily resolution (black) to match the resolution of the altimetry-derived surface currents (ADSC) field. The Lagrangian velocity at each daily location is calculated as the distance between the location 12 hr before the daily location and the location 12 hr after, divided by 24 hr. The nearest grid cells of the Eulerian product (blue dots with red edges) are determined along the Lagrangian trajectory and the velocity at those points is compared to the Lagrangian velocity. The grey areas represent the coastline, and the contours represent the bathymetry.

The point-wise method consists of extracting the velocities of the gridded Eulerian field along the Lagrangian trajectories (Fig. 1) and comparing it to the Lagrangian velocities. It is often the case that the Lagrangian data have a higher temporal resolution than the Eulerian field. We recommend first averaging the higher resolution data to the lower resolution. This avoids interpolating/downscaling the Eulerian field to fit the Lagrangian data.

From this direct comparison, a range of variables can be considered. These include the meridional and zonal velocities, the velocity magnitude or the velocities rotated according to a geographic feature such as a coastline or shelf. In studies of the shelf, the latter involves calculating an along- and across-shelf coordinate system, with the goal of assessing how the velocity field moves independently from the shape of the bathymetric gradients at the coastline and shelfbreak. In this example, the velocities are rotated by an angle that varies at each location and is determined by connecting a straight line between the Lagrangian instrument location and the closest point of a bathymetric contour indicative of the shelfbreak. The along-shelf angle would be perpendicular to the across-shelf angle. It is often necessary to smooth these bathymetric features prior to calculating these angles.

https://doi.org/10.5194/egusphere-2022-1450
Preprint. Discussion started: 23 December 2022

For each component evaluated, the velocity timeseries extracted from the Eulerian field is compared to the Lagrangian velocities. Various analysis and diagnostics can then be applied to compare the Eulerian velocity timeseries to the Lagrangian one. The standard deviation, the root-mean-square error or the correlation coefficient are a few examples. If the time series is sufficiently long, the frequency spectrum of velocity can be computed to compare the frequencies of motion in both velocity fields.

2.2 Eulerian gridding of Lagrangian velocities

The Eulerian gridding consists of mapping the Lagrangian data into a Eulerian gridded field. The gridded field is obtained either by averaging Lagrangian velocities in geographical bins (LaCasce, 2008) or interpolating all Lagrangian data surrounding a location to a cell. Various methods of interpolation can be used to determine the values of the cell such as linear interpolation, optimal interpolation, variational methods etc. The average of the observations inside the cell also corresponds to an interpolation method if it is used with a filter that eliminates data farther than a certain distance from the center of the cell.

Rather than the classical averaging of all Lagrangian devices available together in the same grid, we propose an alternative method that corrects for the number of data points reported in a given area by slowly and quickly moving instruments. Otherwise, slow instruments have more position points in each bin and thus exert a stronger influence on the average.

To perform the mapping (Fig. 2), we first determine the grid that will be used and its resolution $(\Delta x, \Delta y)$. Second, we proceed sequentially through each individual device and produce a unique gridded map based on data from a single device. For each Lagrangian trajectory s, all the cells are scanned to check if the device has passed inside. If the device has not passed through the cell, it is left empty. Otherwise, all velocities within the cell are averaged. This average can be weighted to attribute more weight to the observations close to the center. Different weights can be used, we recommend a Gaussian weight rather than a linear inverse of the distance to avoid the asymptotic weight close to zero. Again, different possibilities exist to parametrize Gaussian weights, a simple choice can be to use the size of the cell.

The grid $\boldsymbol{U}$ obtained for each Lagrangian instrument therefore contains empty cells (where it has not passed) and cells containing the average velocity measured inside (equ. 1). A similar grid D is filled with the average distances from the center of the cells calculated using the same method (equ. 2). This processing is repeated for each of the n devices and the velocities across the devices are averaged together according to their weighted distances from the center of the cell (equ. 3).

Mathematically, this process can be explained by taking $\boldsymbol{u}(s, \boldsymbol{x})$, the velocity of the instrument s at location $\boldsymbol{x} = (x, y)$. The gridded velocity field $\boldsymbol{U}(s, c)$ of the Lagrangian trajectory s at the grid cell c located at $\boldsymbol{x}_c = (x_c, y_c)$ is computed as:

$$\boldsymbol{U}(s,c) = \frac{\sum^{\boldsymbol{x}} \boldsymbol{u}(s,\boldsymbol{x}).q(s,\boldsymbol{x})}{\sum^{\boldsymbol{x}} q(s,\boldsymbol{x})} \tag{1}$$

And the grid of mean distances D is computed as:

$$D(s,c) = \frac{\sum^{\boldsymbol{x}} d(s,\boldsymbol{x}).q(s,\boldsymbol{x})}{\sum^{\boldsymbol{x}} q(s,\boldsymbol{x})} \tag{2}$$

https://doi.org/10.5194/egusphere-2022-1450
Preprint. Discussion started: 23 December 2022

with $\boldsymbol{x} = (x, y)$ and only if $x \in \left[x_c - \frac{\Delta x}{2}; x_c + \frac{\Delta x}{2}\right] \bigcap y \in \left[y_c - \frac{\Delta y}{2}; y_c + \frac{\Delta y}{2}\right]$

$\sum^{\boldsymbol{x}}$ means sum all locations verifying the previous condition (selecting only locations in the cell c), $q(s, \boldsymbol{x})$ is the weight of the location $\boldsymbol{x}$ of instrument s depending on the distance from the center with, as an example, a gaussian weighting like:

$$q(s, \boldsymbol{x}) = exp\left(-\frac{d^2}{0.5\sqrt{(\Delta x)^2 + (\Delta y)^2}}\right) \tag{3}$$

This processing is repeated for each of the n devices and the n grids are finally averaged. For each cell, the average of the n grids in that cell is calculated (equ. 4) and weighted by the averaged distances to the center (equ. 5). The final Eulerian velocity grid $\boldsymbol{\mathcal{U}}$ combines the n grids and thus the trajectories of the n Lagrangian instruments.

$$\boldsymbol{\mathcal{U}}(c) = \frac{\sum_{s=1}^{n} \boldsymbol{U}(s, c).Q(s, c)}{\sum_{s=1}^{n} Q(s, c)} \tag{4}$$

$$Q(s, c) = exp\left(-\frac{D(s, c)^2}{0.5\sqrt{(\Delta x)^2 + (\Delta y)^2}}\right) \tag{5}$$

Usually, the velocity field is not entirely covered by Lagrangian instruments at all times. In these cases of inhomogeneous sampling where, for example, all instruments are deployed around the same spot and sample the region progressively, some events can be missed by the presence of instruments in only one part of the domain. A gridded Eulerian field can therefore be computed using the same methodology as the field derived from Lagrangian devices by only averaging Eulerian velocities when a drifter has passed through the cell. Following this method, n grids are also obtained for the Eulerian product, extracting the velocity from this product at the nearest grid cell from the Lagrangian instrument location or with any interpolation method. The n grids are finally averaged with the same previous methodology. This averaging procedure also accounts for differences in the number of Lagrangian devices between studies – studies that use a lot of Lagrangian data will compare it to a large amount of Eulerian data. However, in the limit of a single Lagrangian instrument, this method converges to the comparison outlined in step #1. Thus, it can be necessary to first assess whether the Lagrangian data sufficiently cover the region of interest before using this progressive averaging method. One way to assess the coverage of data is to compare the gridded Eulerian field following this method to the time-averaged Eulerian field covering all time steps.

The gridded Lagrangian and Eulerian products are then compared to evaluate the differences relative to spatial patterns of velocity and kinetic energy, directions and magnitudes of currents, and even spectra of velocities if the size of the domain allows it.

As pointed out by LaCasce (2008) the choice of bin size in this type of analysis is not trivial. Bins that are too large will smooth out the field and bins that are too small will make the mean very sensitive to eddies and other fine-scale structures. In most of the cases, a convenient choice to facilitate the comparison is to use an identical grid as the original Eulerian gridded products. However, it may be interesting to test a higher resolution to evaluate the induced changes and the impact of gridding.

https://doi.org/10.5194/egusphere-2022-1450
Preprint. Discussion started: 23 December 2022

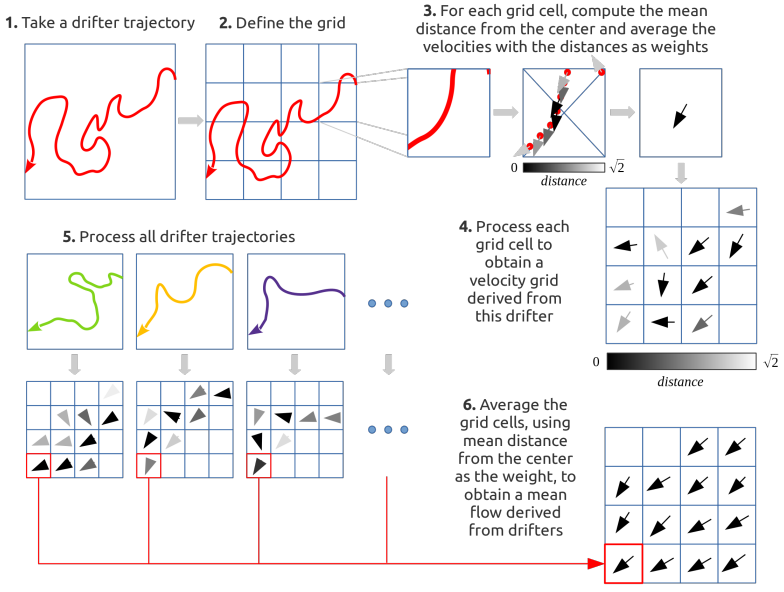

Figure 2. Schematic of the mean flow calculation. This method is intended for Lagrangian instruments, but steps 4-6 can be applied to the evaluated Eulerian product using the velocity at the nearest grid cell and corresponding in time to the Lagrangian location.

The gridding of Lagrangian data performed on the same grid than the Eulerian product and the gridding performed on a higher resolution grid are compared in the same way as the gridded fields from Lagrangian and Eulerian data streams (spatial patterns, direction and magnitudes . . .).

2.3 Observed and synthetic trajectories

The third part of the validation consists of the computation of synthetic Lagrangian trajectories from the gridded Eulerian field (Fig. 3). This corresponds to a conversion of the Eulerian data into the Lagrangian frame of reference. For this, the main idea is to compute a synthetic trajectory by advecting a Lagrangian particle through the Eulerian velocity field (Liu and Weisberg, 2011). The resulting synthetic trajectory must then be compared to the observed trajectory and evaluated using a metric. Various methods could be used such as the distance between the ending points of trajectories, the main direction of trajectories, or a cloud of points, etc. We have found the methodology proposed by Liu and Weisberg (2011) particularly instructive: at each location of the Lagrangian data, a new synthetic particle is released and advected through the velocity field for three days. Then, each three-day trajectory is compared to the actual trajectory over those three days, and a skill score is assessed for each particle launch. This skill score (equ. 6, 7) combines the cumulative distance traveled by observed particles (Lagrangian devices) dl_i and the cumulative separation distance between synthetic and observed particles d_i. It is important to note that this skill score is quite rigorous; to produce a perfect skill score (equal to one), the simulated particle must not only end up at the same location after three days, but also follow the exact pathway to the end point.

https://doi.org/10.5194/egusphere-2022-1450
Preprint. Discussion started: 23 December 2022

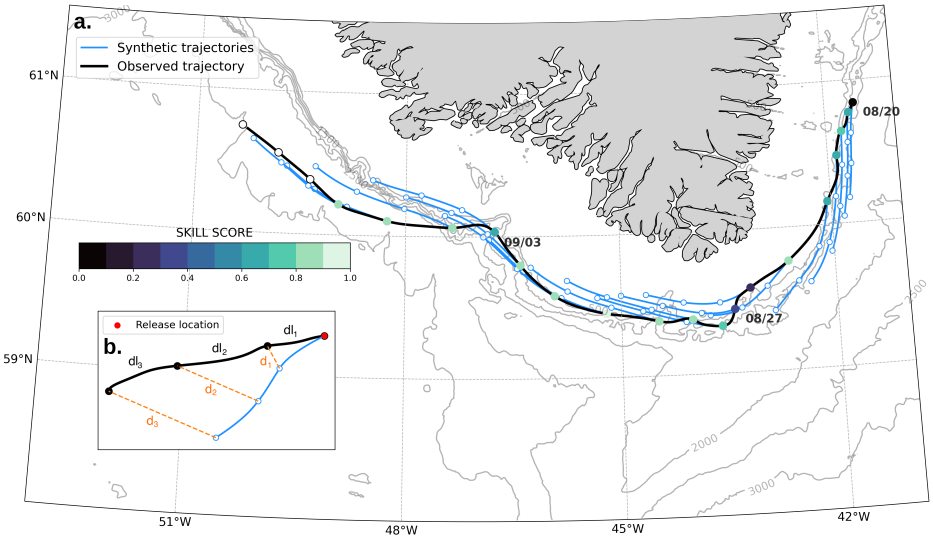

Figure 3. Illustration of the method involving a comparison between observed and synthetic particles using the approach of Liu and Weisberg (2011). (a) Skill scores (colored circles) calculated along a Lagrangian instrument trajectory (black line). Blue lines represent synthetic particle trajectories run over three days. Dot color represents skill score at the daily observed location where the synthetic particle has been released. Grey contours are isobaths. (b) A schematic of the various variables used to calculate the skill score.

$$c = \frac{\sum_{i=1}^{3} d_i}{\sum_{i=1}^{3} (\sum_{j=1}^{i} dl_j)} \tag{6}$$

$$s = \begin{cases} 1 - c, & \text{if } c \leq 1 \\ 0, & \text{otherwise} \end{cases} \tag{7}$$

A disadvantage of this metric is its sensitivity to the duration of the advection of the particles. As proposed by Liu and Weisberg (2011), an evaluation of this sensitivity can be performed in varying the duration to observe the effect on the skill score and determine the most suitable duration. In general, lengthening the duration will induce a better skill score with more statistical significance, but will smooth the spatial differences. Alternative metrics are proposed (e.g., Révelard et al., 2021) and can be used depending on the application, but the original metric remains an interesting first and simple option.

The computation of these synthetic trajectories can be performed using the classical 4th order Runge-Kutta scheme (Hofmann et al., 1991) or using a Lagrangian trajectory simulator (van Sebille et al., 2018).

https://doi.org/10.5194/egusphere-2022-1450
Preprint. Discussion started: 23 December 2022

3 Example Application

We now apply this framework to compare two independent sets of data on surface currents. Surface currents are a particularly important metric to compare because they are useful to a wide range of scientific and operational sub-disciplines. On the scientific side, surface currents can provide a reference velocity to geostrophic shear measurements from moorings, providing referenced geostrophic velocities. And on the practical side, surface currents can be used to aid search and rescue operations (Serra et al., 2020), oil spills, and other debris-related searches (Durgadoo et al., 2021). We also have large data sets of surface velocities that are worth comparing. Indeed, the Global Drifter Program (GDP) produces a large data set of in situ Lagrangian data from surface drifters since the 1980s, and satellite altimeters have produced gridded maps of sea-surface height (SSH) and altimetry-derived surface currents since 1993.

As an application, to test the methodology with a surface current problem, we applied the three steps presented previously to a set of Surface Velocity Program (SVP) drifters to evaluate the accuracy of Altimetry-Derived Surface Currents (ADSC) around Cape Farewell, the southern tip of Greenland. The freshwater from the East Greenland Coastal Current rounding Cape Farewell is a critical component for the climate system because of the proximity to sites of deep open ocean convection that are sensitive to surface density changes. Using the presented methodology, we evaluate the ADSC to check whether it is acceptable to use this very valuable observational data set to study the pathways of freshwater in the region where the observations were historically very sparse and where the discrepancies between modelling studies concerning the shelf-basin exchanges must be investigated.

3.1 Materials and methods

3.1.1 Materials

In August 2021, 38 SVP drifters were released on the southeastern shelf of Greenland (Fig. 4 a) from R/V *Neil Armstrong* (WHOI). These surface drifters are drogued at 15 m with a drogue-to-buoy drag ratio of 40:1 to ensure drifters follow the 15 m current and are not directly pushed by the wind. Two distinct programs provided these drifters: the National Science Foundation (US) funded Greenland Fresh Water Experiment (GFWE) with 12 drifters and the European Research Council (EU) funded Targeted Experiment to Reconcile Increased Freshwater with Increased Convection (TERIFIC) with 26 drifters. The drifters were separated evenly into two batches of 19 drifters that were deployed five days apart (August 15th and 20th). Each batch consisted of one line of four drifters deployed at the shelfbreak, and three zonal lines of five drifters deployed across the inner shelf. The three lines were separated meridionally by 25-30 km between one another, and the drifters along each line were separated by about 5 km (Fig. 4 b, c). The continuous presence of the drogue has been checked using: (1) the buoy parameters, (2) the coefficient of determination R^2 between complex drifter velocity and complex wind velocity (from ERA5, Hersbach et al., 2020) or similarly the least-square complex linear regression of drifter velocity from wind velocity (Kundu, 1976; Poulain et al., 2009). Both methods confirm that all drifters maintained their drogues throughout the period of analysis described in this paper. We also tested whether any of the data points qualify as outliers according to the Elipot et al. (2016) definitions, but we did not identify any. Four of the drifters were trapped in fjords for prolonged periods, thus we did

https://doi.org/10.5194/egusphere-2022-1450
Preprint. Discussion started: 23 December 2022

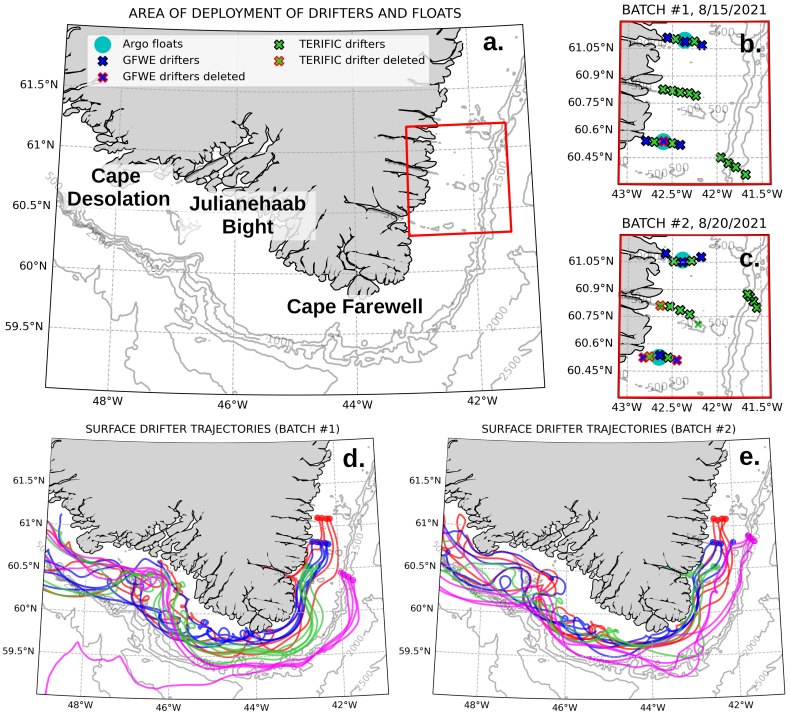

Figure 4. (a) The study region, with Cape Farewell at 44°W, Julianehaab Bight at 46°W and Cape Desolation at 48°W. Contour lines represent isobaths. Deployment location of drifters and floats respectively for first (b , August 15th) and second (c , August 20th) batch. Drifter trajectories respectively for first (d) and second (e) batch. Colors represent lines of drifters.

not consider them. These steps left us with 34 trajectories to analyze. We then filtered out high frequency variability that can be attributed to tides and inertial oscillations by using a 24 hr cut-off low-pass filter. More details on drifter data processing are available in Section 1 and Figures S1 to S3 of the supplementary material.

Two data sets of ADSC have been evaluated in this study. The first is the Copernicus Marine Environment Monitoring Service (CMEMS) near-real time product denominated "Global Ocean Gridded L4 Sea Surface Heights And Derived Variables Nrt". The processing used is the DUACS multi-mission altimeter data processing system DT-2021 (Faugère et al., 2022) provided by CNES/CLS with a methodology detailed in Pujol et al. (2016). The altimetry data is merged from all available altimetry missions and interpolated on a 1/4° grid with a daily resolution. The geostrophic currents provided in this data set benefit from the CNES-CLS18 Mean Dynamic Topography (MDT) product (Mulet et al., 2021). This MDT gathers altimetry, gravity and drifter data. It shows better results in all regions around the globe compared to the previous product CNES-CLS15 especially in coastal areas. The geostrophic currents are computed using a nine-point stencil width methodology (Arbic et al., 2012). In the following work, we refer to this data set as "Geostrophy".

The second ADSC data set is the "Global Total Surface and 15m Current (COPERNICUS-GLOBCURRENT) from Altimetric Geostrophic Current and Modeled Ekman Current Processing". The Ekman velocities at 15 m depth are computed from

https://doi.org/10.5194/egusphere-2022-1450
Preprint. Discussion started: 23 December 2022

ERA5 (Hersbach et al., 2020) 3h wind data following the methodology developed in Rio and Hernandez (2003), Rio et al. (2011), Rio (2012) and Rio et al. (2014). An empirical Ekman spiral-like model is estimated, based on 2 parameters determined from a least-squares regression from SVP drifters' data, Argo floats data and wind stress measurements from ECMWF ERA5. The field denominated in this work as"Geostrophy+Ekman" is then the addition of Ekman contribution to the previous geostrophic current data set. The final product provides a 6-hour frequency data set with zonal and meridional components of surface velocity. For fair comparison with the daily Geostrophy product, here we primarily evaluate daily velocities but have also looked at the 6-hour frequency product to see the impact of higher temporal resolution. The 15 m depth velocities are used for consistency with 15m depth drogued drifter.

In addition to the two ADSC data sets, we also compare the drifter velocities to the "Arctic Ocean Physics Analysis and Forecast" product from the operational TOPAZ4 Arctic Ocean system (Sakov et al., 2012). This is a completely different data set in that it assimilates all possible data streams (e.g. Argo, satellites) rather than only relying on satellite altimetry and wind products. The goal of including TOPAZ in the first step of this methodology is to provide context to the results with ADSC data sets. This data assimilation product is based on the HYCOM model and a 100-member Ensemble Kalman Filter (EnKF) assimilation scheme.

3.1.2 Methods

The point-wise method has been performed on drifter daily velocities to extract the collocated and contemporaneous velocities from the ADSC. Four components of the velocities have been computed: the zonal (u), the meridional (v), the along-shelf, and the across-shelf velocities. In parallel, a time series of velocity has been extracted along each drifter trajectory from the ADSC and TOPAZ. We compare, on these time series, the standard deviation (normalized by drifter velocity standard deviation $\hat{\sigma_f}$), the correlation coefficient r relative to the drifters' daily velocities, the root-mean-square error (RMSE) and the percent variance explained (equ. 8).

$$\text{Variance of X explained by Y } (\%) = 100 \times \left[1 - \left(\frac{\sigma^2(X-Y)}{\sigma^2(X)}\right)\right] \tag{8}$$

In this analysis, the TOPAZ4 reanalysis product serves as a reference to which the ADSC results can be compared. Taylor diagrams and skill scores S (equ. 9) (Taylor, 2001) are used to concatenate all statistics.

$$S = \frac{4(1+r)}{(\hat{\sigma_f} + 1/\hat{\sigma_f})^2.(1+r_0)} \tag{9}$$

with r_0 the maximum expected correlation coefficient (here taken equal to one).

In the second step of the methodology, the velocities from the surface drifters are mapped onto a Eulerian grid that has the same 1/4° grid as the ADSC. A separate grid is constructed for each of the 34 drifters and then averaged together to produce a single mapped velocity field from the drifters. The same process is then applied to ADSC to compute mean flows synchronous with drifter sampling. The general patterns of the different mean flows have been compared, the angle between ADSC and

https://doi.org/10.5194/egusphere-2022-1450
Preprint. Discussion started: 23 December 2022

drifters' velocity vectors are determined and finally the ratio ADSC velocities over drifter velocities is computed. The influence of gridding and the consistency of the 1/4° drifter gridding with the original drifter data is evaluated by comparing the results at 1/4° resolution to 1/12°. This higher resolution was chosen to test the sensitivity of the results to the resolution of the grid and ensure that an average of 4 drifters passed through each cell. A higher resolution would imply fewer drifters on average.

Finally, as the third step in the prescribed methodology, synthetic trajectories are run through the ADSC velocity fields. A new particle is initialized at the daily locations of each drifter, and then advected for 3 days. The skill score from Liu and Weisberg (2011) (equ. 6 and 7) is applied at each trajectory to assess their consistency and plotted on a map at the released location. The sensitivity of the skill scores to the duration of the particles' advection is evaluated by repeating the experiment with various durations spanning from 2 to 14 days.

3.2 Results

3.2.1 Applying the point-wise comparison to surface drifters and ADSC around Cape Farewell

We present here the results of the point-wise comparison between the surface drifters and ADSC around Cape Farewell. Figure 5 shows the Taylor diagrams of the evaluated products (ADSC and TOPAZ4). Differences between high scores are visually accentuated in order to detail differences between the products. Meridional velocities (v) are well resolved by altimetry-derived products (Fig. 5 b) with an average skill score of 0.87 computed from the average correlation coefficients of 0.75 (Geo.) and 0.79 (Geo.+Ekman) and the average normalized standard deviations of 0.84 (Geo.+Ekman) and 0.92 (Geo.). The zonal component (u) has lower scores overall (Fig. 5 a) with average skill scores of 0.63 (Geo.) and 0.69 (Geo.+Ekman) computed from the average correlation coefficients of 0.62 (Geo.) and 0.64 (Geo. + Ekman) and the average normalized standard deviations of 0.60 (Geo.) and 0.65 (Geo.+Ekman). This difference in scores between the u and v components can be explained by the shape of the coast that makes meridional velocities easier to reproduce. As the drifters follow the shelf around Cape Farewell the meridional velocities shift from high negative velocities (southward) to positive velocities (northward). If the gridded Eulerian product simulates this general behavior, i.e. the current follows the bathymetry, then the skill scores of the meridional velocities will be higher. Another potential explanation of this difference is that sea surface height gridded at 1/4° used to compute geostrophic currents, does not have the same spatial resolution in latitude and in longitude. A degree of latitude corresponds always to the same distance, $\approx$ 111 km, but a degree of longitude at 60°N corresponds to half the latitudinal resolution, or 55 km. In a 1/4° product, the grid cells are 27 km in latitude, and 13 km in longitude. The Rossby Radius in this region is on the order of 10 km, thus the 1/4° product approaches the Rossby Radius in longitudinal span. Meridional geostrophic velocities, computed as $v_g = \frac{g}{f}\frac{\partial \eta}{\partial x}$, benefit from the better longitudinal resolution. The difference between altimetry-derived velocity and reanalysis product is very important for meridional velocities, though it should be noted that the velocities in TOPAZ4 do not experienced such improvement from u to v (average skill score for zonal component is 0.59 and for meridional, 0.60).

The along and across-shelf velocities present lower average skill scores (Fig 5 c and d), respectively 0.51 (Geo.), 0.60 (Geo.+Ekman) and 0.60 (Geo.), 0.64 (Geo.+Ekman). This decrease from u and v to along-shelf and across-shelf velocities is due to fact that coordinate system follows the bathymetry and thus only considers variability distinct from the bathymetric

https://doi.org/10.5194/egusphere-2022-1450
Preprint. Discussion started: 23 December 2022

contours. To first order, the drifters flow along the shelf from the east to the west, such that only positive along-shelf velocities are experienced. Alternatively, the across-shelf velocities can be positive or negative but cover a smaller range of possible values. The particles following the coastal current are constrained by the conservation of potential vorticity to remain on the shelf, therefore the across-shelf velocity is much smaller than the along-shelf, zonal or meridional velocities. Nevertheless, the across-shelf Taylor diagram shows that Geostrophy+Ekman performs better than other products especially compared to Geostrophy only.

The RMSE obtained for each velocity component shows very good results for Geostrophy compared to the reanalysis product, especially for meridional, along-shelf and across-shelf components (Fig. 5 e). The RMSE was much lower for the across-shelf component especially compared to the along-shelf one – the across-shelf velocities are often difficult to model with geostrophy alone and thus the expectation is that the error would be higher. However, this lower RMSE could be explained by the smaller magnitude of the across-shelf velocities which make the lower RMSE worse relatively to the magnitude of the velocity component. This hypothesis is reinforced by the percent variance explained (Fig. 5 f) that normalizes these errors by the total amount of variance in each direction. When the amount of total variance is accounted for, the along-shelf and across-shelf metrics are similar, and the difference between the u, v fields and the along and across-shelf velocities is accentuated. In addition, the effect of the Ekman component is more apparent in the percent variance explained plot. In the along-shelf direction, the addition of the Ekman component nearly doubles the percent variance explained. Similarly, in the across-shelf direction, the Ekman component makes an important contribution but surprisingly, the change in percent variance explained when the Ekman component is added is larger in the along-shelf direction than the across-shelf direction. Given that the flow along bathymetric contours (along-shelf direction) is largely thought to be geostrophic, while any deviations to it (the across-shelf direction) is ageostrophic, it is surprising that the Ekman component is more important in the along-shelf velocities than the across-shelf velocities. The Ekman component can influence the along-shelf currents by winds that are misaligned with the currents. This misalignment occurs frequently in the vicinity of Cape Farewell as the dominant wind patterns are no longer constrained by the topography of Greenland and the winds cross the shelf. Thus there is good reason for why the Ekman contribution is surprisingly large in the along-shelf direction.

The Geostrophy+Ekman data set are also available at 6-hour frequency due to the higher frequency wind products, so we also investigated the difference between the 6-hourly data and the 6-hourly drifter data. Recall that we chose the daily Geo.+Ekman data for more direct comparison to the Geostrophy only fields, which are only available at daily resolution. The 6-hourly Eulerian data compared to 6-hourly drifter data have comparable correlation coefficients but weaker normalized standard deviations than the other altimetry-derived products. This data set has also a larger RMSE (Fig. 5 e) but the percent variance explained is close to the daily data. Two parameters affect this comparison simultaneously: the higher temporal resolution of the Geostrophy+Ekman 6-hourly field that should imply a better accuracy and also the higher temporal resolution of the drifter data to which the Eulerian data are compared that contains more variability than the daily drifter data. The 6-hour data is therefore likely more realistic, but the drifters' motion is also more variable at this shorter temporal scale and thus more difficult to reproduce.

https://doi.org/10.5194/egusphere-2022-1450
Preprint. Discussion started: 23 December 2022

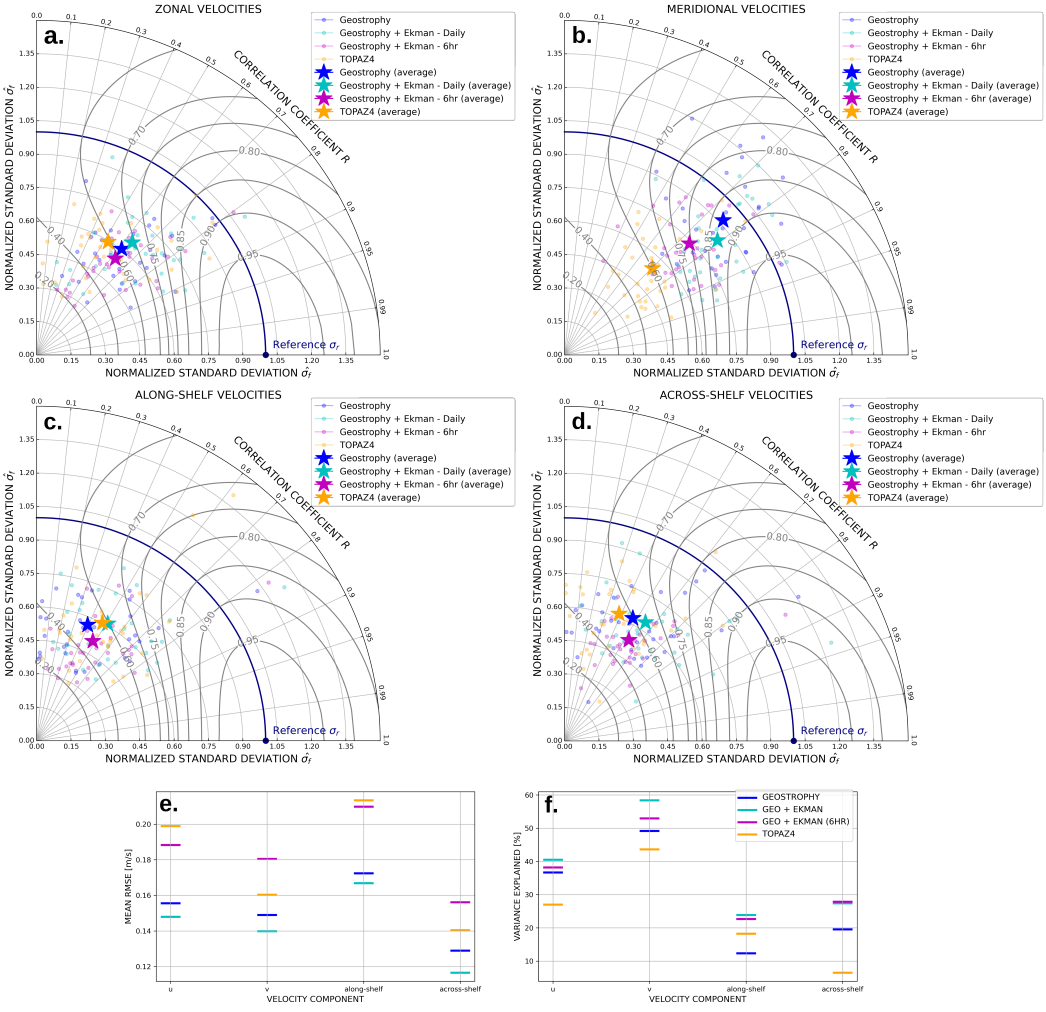

Figure 5. Taylor diagrams of the point-wise comparison between the surface drifter velocities and either ADSC or TOPAZ4 for the (a) zonal, (b) meridional, (c) along-shelf and (d) across-shelf components. The x and y axes depict the normalized standard deviation (ratio of ADSC's standard deviation to surface drifter's standard deviation). Polar coordinates represent the correlation coefficient between product and drifter timeseries. Contours represent Taylor Skill Scores. Each trajectory for each product is represented with a point. The stars represent the average across all 34 trajectories of normalized standard deviations and correlation coefficients for each product. Note the non-linearity of scales used for correlation and skill score contours in the figure. The Taylor diagrams are modified versions of an initial Python code by Copin (2012). (e) Root mean square error (RMSE) for each velocity component. (f) Percentage of variance explained for each velocity component.

https://doi.org/10.5194/egusphere-2022-1450
Preprint. Discussion started: 23 December 2022

3.2.2 Eulerian gridding of surface drifter velocities and ADSC

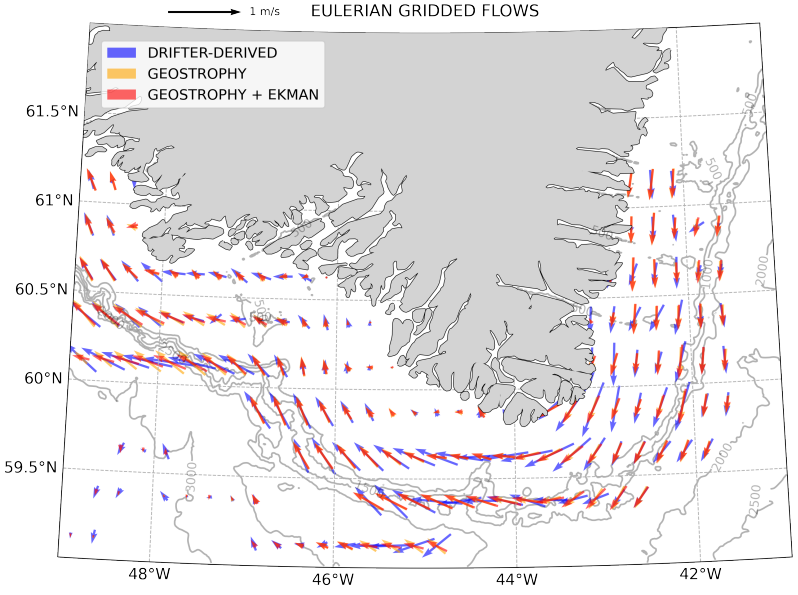

Figure 6. Gridded surface currents derived from drifter data (blue), Geostrophy product (yellow) and Geostrophy+Ekman product (orange).

The drifters, Geostrophy and Geostrophy+Ekman products have been gridded using the method prescribed above in section 2.2. The vector map (Fig 6) shows that drifters mainly sampled the shelf around Cape Farewell. The general visual consistency between remote-sensing products and drifter-derived field is also very good. From a spatial pattern point of view, the along-shore current and the detachment of the coastal current from the coast at Cape Farewell are clearly visible and represented in all fields. To investigate more specifically this consistency, two quantities have been computed at each grid point: (1) the angle between the ADSC and the drifter-derived velocities and (2) the ratio of the ADSC over the drifter-derived velocities.

On the maps presenting angles between drifter velocities and ADSC directions (Fig 7 a and b), the angles are very small over most of the domain (smaller than 20°) especially close to the shelfbreak where the direction of currents is a key point to resolve the shelf-basin exchanges. Some grid points very close to the coast present larger angles (larger than 60°) but only few drifters passed inside these cells and the statistical significance is therefore smaller. The average angle over the region, weighted by the number of drifter traveling the cells, is very small: 14.5° for Geostrophy only and 12.3° by adding Ekman. It highlights the particularly good ability of ADSC to reproduce the direction of currents.

The maps showing velocity ratios (Fig. 7 c and d) depict areas of strong under and overestimation. The regions south of Cape Farewell and Cape Desolation are showing underestimation of about 50%, indicating that the ADSC fields have trouble resolving the zonal velocity in the coastal current. Again, this result is likely due to the large meridional separation between 1/4° grid cells, that can be easily visualized in Fig. 7. Importantly, the magnitude of this error drops significantly at the shelfbreak, which is the key component for representing flux between the shelf and the ocean basin. So while the coastal current is likely

https://doi.org/10.5194/egusphere-2022-1450
Preprint. Discussion started: 23 December 2022

not well-resolved south of Cape Farewell, the shelfbreak jet remains present. The mean absolute errors observed is 37.2% for Geostrophy and 35.6% for Geostrophy+Ekman. These percentages capture the magnitude of the errors, both in underestimation and in overestimation.

The difference between Geostrophy and Geostrophy+Ekman is small in these averaged fields. Indeed, the mean angle between the vectors is around 5.2° (Fig. 7 e) and the mean difference between velocities (Fig. 7 f) is about 7.1% of Geostrophy+Ekman velocities. The main area where directions are different is on the West Greenland Shelf, around Cape Desolation with differences up to 12-15°. Alternatively, we observe two hot spots where the magnitudes of velocities are different: South-East of Cape Farewell where Ekman contribution increases the magnitudes and North-West of Cape Farewell, around Julianehaab Bight, with Ekman contribution decreasing them.

The ADSC seem able to reproduce the current's direction with high accuracy, but the magnitude is strongly underestimated. We suggest that this underestimation is due to the gridding of the along-track altimetry data that smoothes the velocities, and likely underestimates their true variance. On the shelfbreak the direction and the magnitude of currents is well resolved, which seems to indicate a good ability of ADSC to represent shelf-basin exchanges. The Ekman contribution seems to be a small contribution to the total velocity but improves both direction and magnitude consistently in both the along-shelf and across-shelf directions.

We compare 1/12° to 1/4° to evaluate the differences due to change in resolution (Fig 8). The 1/12° velocity grid shows more details and small-scale features (a). This product identifies the very strong velocity regions on the shelf south of Cape Farewell and on the shelfbreak south of Cape Desolation. Current direction and magnitude seem consistent and the mean kinetic energy (b, d) and eddy kinetic energy (c, e) fields show close values in general and in the energy hot spots as well. The 1/4° resolution therefore gets the right values at the right locations. In general, this exercise in testing various spatial resolutions of the gridded surface drifter velocity fields has shown us that future improvements to the gridded altimetry record from higher resolution products and the SWOT mission will likely improve the comparisons to the surface drifter velocities and allow for more detailed studies of the circulation structure, but surprisingly, the 1/4° gridded fields capture the majority of the circulation features important to the shelf-basin exchange in this region.

In this section, we presented a methodology to compute mean flows from gridded Eulerian fields that closely simulates the progressive sampling of the domain by the surface drifters, so that the gridded Eulerian fields are averaged in the same spatial/temporal domain as the drifters. We also evaluated how sensitive this result is using a simple time average of the gridded Eulerian fields. Figure S4 (supplementary material) compares the Geostrophy and Geostrophy+Ekman velocity fields computed with these two different methods. They yield very similar fields, except in the region near the shelfbreak south of Cape Desolation. In this region, Geostrophy+Ekman computed with the 'drifter following' methodology clearly differs from the other fields. In our example, the methodology does not change much for Geostrophy only data set and the time averaged Geostrophy+Ekman field is very close to those Geostrophy fields. This could indicate that the Ekman contribution diminishes when averaged over a long enough period of time in this region where the synoptic storm time scale is around 5 days. The short time scale wind events likely play a role for the cross-shelf exchange as highlighted by the vector field obtained with the 'drifter following' method.

https://doi.org/10.5194/egusphere-2022-1450
Preprint. Discussion started: 23 December 2022

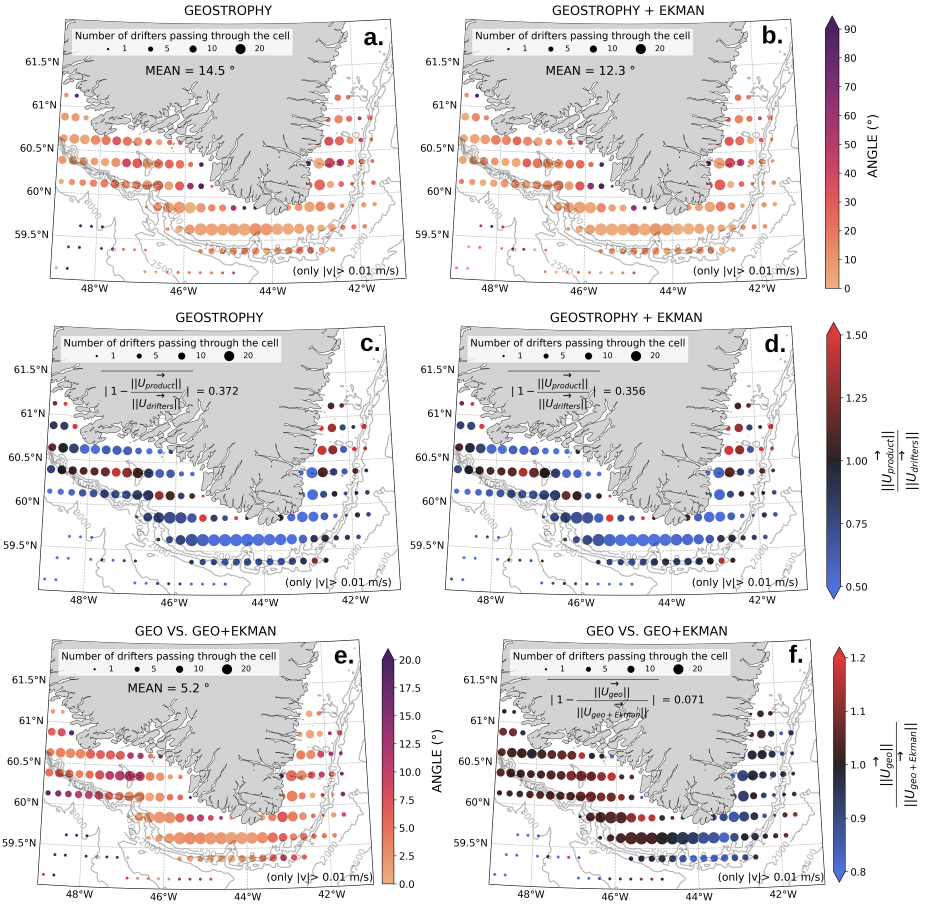

Figure 7. Differences in angle (a, b) and magnitude (c, d) between surface drifter velocities and Geostrophy (a, c) and Geostrophy+Ekman (b, d) velocities. In panels a and b, color represents the angle and size of dots represents the number of different drifters passing through a cell. Only velocities greater than 1 cm/s are considered to ignore the error due to random characteristics of vectors with small magnitudes. The mean corresponds to the average angle over the dots weighted with the number of drifters passing in a cell. In panels c and d, color represents the ratio of ADSC over surface drifter velocities. Size of dots represents the number of different drifters passing through a cell. Score written in the figure corresponds to the mean absolute error weighted with the number of drifters passing in the cells. The bottom row (e, f), depict the differences in magnitude and angle between the Geostrophy and Geo.+Ekman velocity vectors. Note the different color scales for these two panels than the top four.

https://doi.org/10.5194/egusphere-2022-1450
Preprint. Discussion started: 23 December 2022

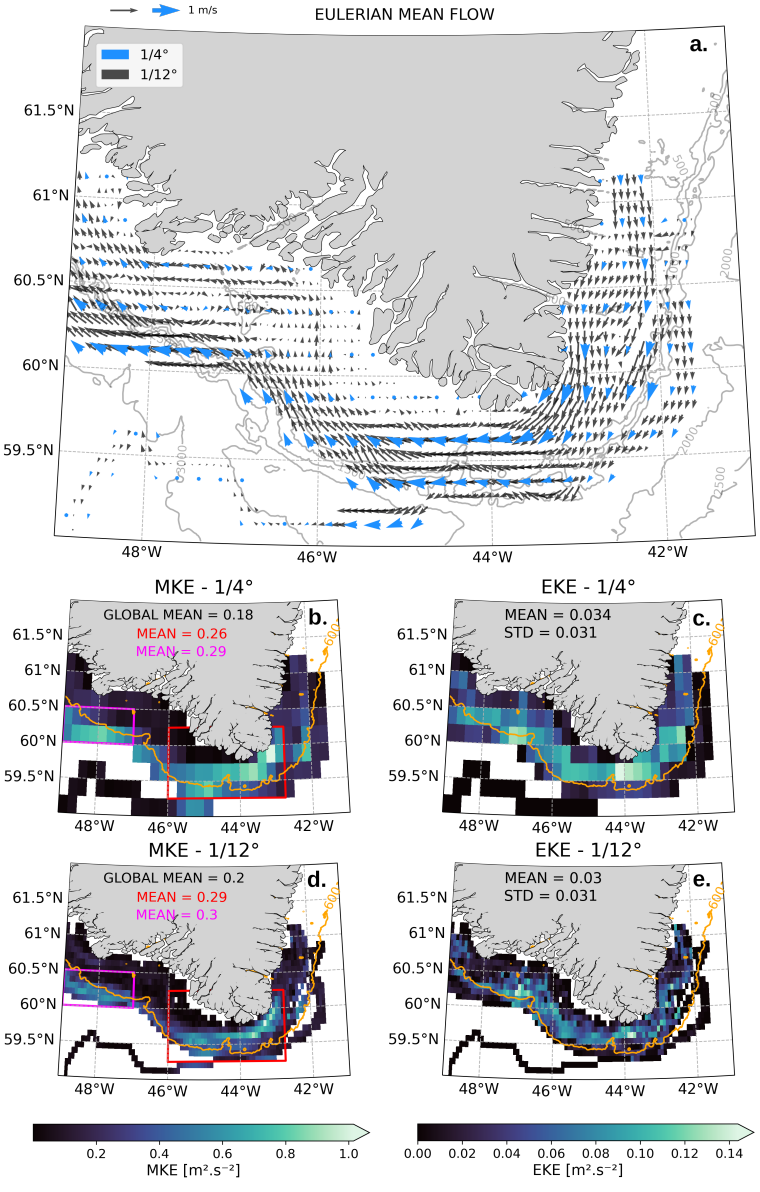

Figure 8. Comparison of gridded flows derived from drifter trajectories with varying resolution. (a) Comparison of 1/4° (blue) and 1/12° (black) vectors. Mean Kinetic Energy (MKE) maps obtained on 1/4° (b) and 1/12° (d) grids. Eddy Kinetic Energy (EKE) maps obtained on 1/4° (c) and 1/12° (e) grids. Values provided in panels b-e are the means over the color-coded boxes.

https://doi.org/10.5194/egusphere-2022-1450
Preprint. Discussion started: 23 December 2022

3.2.3 Observed and synthetic trajectories around Cape Farewell

ADSC velocities are now evaluated in the Lagrangian frame by applying the methodology described in section 2.3 and originally designed by Liu and Weisberg (2011). The sensitivity of the skill scores to the duration of the particles' advection has been tested in repeating the experiment with various durations (from 2 to 14 days). We chose to use 3 days as proposed by Liu and Weisberg (2011) so that we could compare our values to theirs, as well as to avoid too short experiments which could be insignificant and too long where local information would be lost. Liu et al. (2014) applied this methodology to the evaluation of various remote-sensing product in the Gulf of Mexico and found a mean skill score of 0.50 in the open ocean and 0.41 on the shelf. The ADSC data they used were a combination AVISO (delayed time) + Rio2009 (MDT) + Ekman, which corresponds to the "Geostrophy + Ekman" product evaluated in our work. When the Ekman component is removed from their ADSC product, the open ocean skill score does not change but the shelf one decreases to 0.35. We can use their results as a reference to interpret the results obtained in the present work.

Here, the vast majority of our drifters traveled on the shelf, and we calculate a mean skill score of 0.47 for Geostrophy only and 0.50 for Geostrophy+Ekman. Our skill scores on the shelf with the Ekman component (0.50) exceed the Liu et al. (2014) skill scores on the shelf (0.41) and are comparable to those obtained in the open ocean. Without Ekman, the mean score obtained with data mainly located on the shelf is 0.47 while the mean score from Liu et al. (2014) without Ekman was only 0.35 on the shelf and 0.50 on the open ocean. There is also a clear spatial signal in the skill scores (Fig. 9), with an area of lower skill scores (red hatch) around Julianehaab Bight. These seem to correspond to the area of slowly eddying shelf flow described by Duyck and De Jong (2021). The average skill score associated is 0.38 for Geostrophy and 0.39 for Geostrophy+Ekman. This turbulent area, supposed to be more difficult to be reproduce because of its particular dynamics, shows almost similar results than Liu et al. (2014) with Ekman contribution on the shelf and even better results comparing to Geostrophy only. The rest of the shelf shows particularly high mean skill scores with 0.55 for Geostrophy only and 0.58 with Ekman contribution. The results obtained here with the remote-sensing products are thus particularly good, especially considering Ekman contribution. The impact of this contribution on the skill score is investigated by computing the difference between score obtained with both products (Fig. 9 c). Ekman contribution improves the main skill score by 0.03 and large improvements appear particularly on the East Greenland shelf for trajectories not located against the coast and south of Cape Desolation close to the coast.

From those results, we conclude that ADSC seem able to reproduce the trajectories of surface drifters in the region of Cape Farewell. By extension, we expect a good ability to reproduce water masses displacement. ADSC could therefore be used to investigate pathways and fate of fresh water.

We expect the skill scores to be better for the open ocean than the shelf because the scales of motion are larger in the open ocean and the flow is more geostrophic. Thus, it is impressive that the skill scores found on the shelf in the current study are comparable to the open ocean skill scores from Liu et al. (2014). Furthermore, our study is at higher latitudes where the Rossby Radius of Deformation is smaller and thus the comparison of skills scores would favor more southerly latitudes. However, the tracks of polar orbiting altimeters converge at high latitudes so there is better along-track coverage, and we are also using an

https://doi.org/10.5194/egusphere-2022-1450
Preprint. Discussion started: 23 December 2022

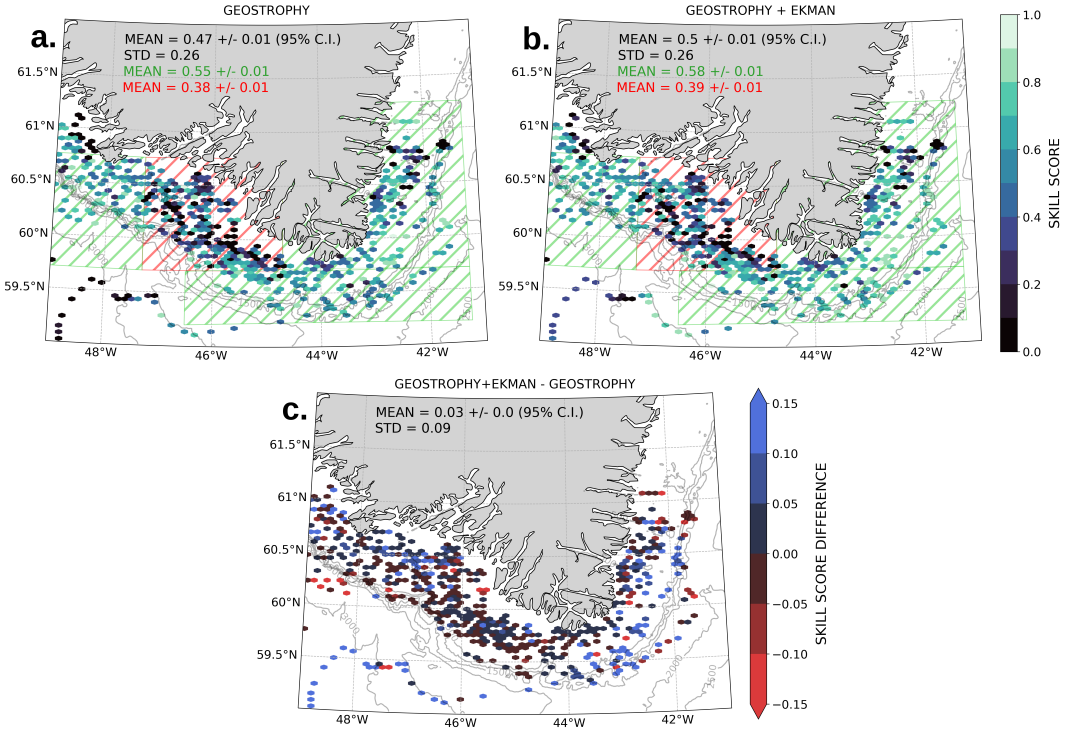

Figure 9. Synthetic trajectories evaluation for Geostrophy (a) and Geostrophy+Ekman (b). Dots represent daily locations of drifters and colors represent the score obtained for the trajectory computed with the 3 following days. An area presenting lower scores is hatched in red and the rest of the shelf with higher skill scores is hatched in green. Confidence intervals are computed using Bootstrap methodology. (c) Skill score difference due to Ekman contribution with blue denoting an increase in skill score when the Ekman velocities are included, and red denoting a decrease.

updated MDT data set in our analysis (2009 version of the CNES-CLS MDT compared to the 2018 version), both of which could contribute to this favorable comparison of our results.

4 Conclusions

The altimetry-derived surface currents are remarkably capable of recovering the spatial structure of the flow field on the South Greenland Shelf and can mimic the Lagrangian nature of the flow as observed from surface drifters. This good agreement is especially strong for the meridional velocities, likely due to the strong bathymetric constraints and the meridional orientation of the shelf in the area, as well as the higher spatial resolution in the zonal dimension of the gridded altimetry product. The Taylor skill scores drop for the zonal velocity and the along-shelf and across-shelf velocities, but they remain high considering that the shelf coordinate system accounts for the bathymetric steering of the flow. So, the skill scores for these latter two velocity components are essentially estimating how well the flow field is characterized beyond the bathymetric control, and thus the

https://doi.org/10.5194/egusphere-2022-1450
Preprint. Discussion started: 23 December 2022

skill scores are quite high given that assumption. ADSC show a particular ability to reproduce the direction of currents around Cape Farewell with errors on directions around 12° to 14° in average, depending on the product used.

Overall, the addition of the Ekman velocities to the Geostrophic product improved the comparisons, though not by as much as originally hypothesized and not for specific velocity components. It is likely that during high wind events this Ekman component is more noteworthy. Though our drifter observations were limited to a relatively short period in August and September of 2021, when winds are at their climatological minima, we note that the conditions experienced during this period in August and September of 2021 were noteworthy for their strong winds for this time of year. The drifters directly sampled upwelling and downwelling on the East Greenland Shelf, as well as upwelling on the West Greenland Shelf. Finally, the simulations of particle trajectories highlight the particularly good ability of ADSC to mimic the displacement of surface drifters in the region and by extension the displacement of water masses.

The main sources of error between the ADSC and the surface-derived velocities lie in the magnitude of velocities, especially the zonal velocities around the southernmost tip of Greenland. Here, the direction of the flow is well constrained, but the magnitude is about half of the observed velocity. This result is concerning, though the direction of the vectors remains on the shelf, and the direction and magnitudes are well-resolved at the shelfbreak. As the shelfbreak circulation is critical for evaluating shelf-basin fluxes, we remain confident that the ADSC are doing a good job of tracking this exchange. Interestingly, the gridded products (step #2 in the methodology) seem to imply that the ADSC would be better suited to tracking the shelf-basin exchange than the exchange from the coastal current to the shelfbreak currents. But the Lagrangian simulations (step #3 in the methodology) imply that the ADSC are quite good on the SE Greenland Shelf, where we observe quite a bit of coastal current-to-shelfbreak exchange, especially under the initial upwelling-favorable winds. Thus, we conclude that the ADSC are good at tracking the shelf-basin exchange, and one should specify exactly what is of interest in the coastal current-to-shelfbreak exchange prior to using the ADSC fields. Overall, we gained significant confidence in ADSC around the southern tip of Greenland through this example application. Though our initial 'null hypothesis' was that the ADSC would have trouble resolving the shelf circulation, the common result across all three steps of this proposed methodology was that the ADSC were capturing critical components of the circulation..

A large caveat of our results here has been that these results are specific to a roughly two-week period in Aug/Sep 2021 and may or may not be representative of the longer-term variability. To address this concern, we used a database of 34 drifters from the 6-hourly data set (Lumpkin and Centurioni, 2019) derived from Global Drifter Program (GDP) data that crossed onto the shelf from 1993-2021 (Supplementary Material Section 2). The results from extending the temporal scope show a good coherence between surface drifters' trajectories and altimetry-derived surface currents from 1996 to 2020 in all seasons investigated, leading us to believe that this good correspondence is not specific to our brief study period, albeit with limited data to test. How far back in time one can reliably reconstruct the shelf circulation with ADSC, specifically as the number of altimeters decreases significantly prior to 2000, remains to be answered.

https://doi.org/10.5194/egusphere-2022-1450
Preprint. Discussion started: 23 December 2022

Acknowledgements. This work was funded by the National Science Foundation grant number 2047952. TERIFIC was funded from the European Research Council (ERC) under the European Union's Horizon 2020 research and innovation programme (grant agreement No 803140). The authors would like to thank Lucas Drumetz, Eleanor Frajka-Williams, Renske Gelderloos, Christophe Maes, Bob Pickart, Florian Sévellec and Pierre Tandeo for their input and guidance during this project.

Code availability. The python codes to implement the presented methodology are available on the "ADSC-SVP-Comparison" repository (https://github.com/arthurarsene/ADSC-SVP-Comparison).

Data availability. The surface geostrophic current data set "Global Ocean Gridded L4 Sea Surface Heights And Derived Variables Nrt" is publicly available on the Copernicus Marine Service CMEMS website (https://doi.org/10.48670/moi-00149). The version including Ekman contribution named "Global Total Surface and 15m Current (COPERNICUS-GLOBCURRENT) from Altimetric Geostrophic Current and Modeled Ekman Current Processing" is also available on this website (https://doi.org/10.48670/moi-00049). Finally, CMEMS website also provides TOPAZ4 (Sakov et al., 2012) reanalysis in open access (https://doi.org/10.48670/moi-00001). "Global Drifter Program quality-controlled 6-hour interpolated data" from Lumpkin and Centurioni (2019) are publicly available (https://www.aoml.noaa.gov/phod/gdp/interpolated/data/all.php). The comparison with GDP data has been perfored on the reprocessed versions of altimetry-derived surface currents available on CMEMS as "Global Ocean Gridded L 4 Sea Surface Heights And Derived Variables Reprocessed 1993 Ongoing" (https://doi.org/10.48670/moi-00148) and "Global Total Surface and 15m Current (COPERNICUS-GLOBCURRENT) from Altimetric Geostrophic Current and Modeled Ekman Current Reprocessing" (https://doi.org/10.48670/moi-00050). The deployed drifters from GFWE and TERIFIC are in the process of being incorporated in the GDP data set at the moment of submitting this manuscript.

Author contributions. AC conducted the analysis and co-wrote the manuscript. NPF devised the study and co-wrote the manuscript.

Competing interests. The authors have no competing interests to disclose.

https://doi.org/10.5194/egusphere-2022-1450
Preprint. Discussion started: 23 December 2022

References

Arbic, B. K., Scott, R. B., Chelton, D. B., Richman, J. G., and Shriver, J. F.: Effects of stencil width on surface ocean geostrophic velocity and vorticity estimation from gridded satellite altimeter data, Journal of Geophysical Research: Oceans, 117, https://doi.org/10.1029/2011JC007367, _eprint: https://onlinelibrary.wiley.com/doi/pdf/10.1029/2011JC007367, 2012.

Copin, Y.: Taylor diagram for python/matplotlib, https://doi.org/10.5281/zenodo.5548061, language: eng, 2012.

Durgadoo, J. V., Biastoch, A., New, A. L., Rühs, S., Nurser, A. J., Drillet, Y., and Bidlot, J.-R.: Strategies for simulating the drift of marine debris, Journal of Operational Oceanography, 14, 1–12, https://doi.org/10.1080/1755876X.2019.1602102, publisher: Taylor & Francis _eprint: https://doi.org/10.1080/1755876X.2019.1602102, 2021.

Duyck, E. and De Jong, M. F.: Circulation Over the South-East Greenland Shelf and Potential for Liquid Freshwater Export: A Drifter Study, Geophysical Research Letters, 48, e2020JB020 886, https://doi.org/10.1029/2020GL091948, _eprint: https://onlinelibrary.wiley.com/doi/pdf/10.1029/2020GL091948, 2021.

Elipot, S., Lumpkin, R., Perez, R. C., Lilly, J. M., Early, J. J., and Sykulski, A. M.: A global surface drifter data set at hourly resolution, Journal of Geophysical Research: Oceans, 121, 2937–2966, https://doi.org/10.1002/2016JC011716, _eprint: https://onlinelibrary.wiley.com/doi/pdf/10.1002/2016JC011716, 2016.

Faugère, Y., Taburet, G., Ballarotta, M., Pujol, I., Legeais, J. F., Maillard, G., Durand, C., Dagneau, Q., Lievin, M., Roman, A. S., and Dibarboure, G.: DUACS DT2021: 28 years of reprocessed sea level altimetry products, Tech. Rep. EGU22-7479, Copernicus Meetings, https://doi.org/10.5194/egusphere-egu22-7479, conference Name: EGU22, 2022.

Haine, T. W. N., Gelderloos, R., Jimenez-Urias, M. A., Siddiqui, A. H., Lemson, G., Medvedev, D., Szalay, A., Abernathey, R. P., Almansi, M., and Hill, C. N.: Is Computational Oceanography Coming of Age?, Bulletin of the American Meteorological Society, 102, E1481–E1493, https://doi.org/10.1175/BAMS-D-20-0258.1, publisher: American Meteorological Society Section: Bulletin of the American Meteorological Society, 2021.

Hersbach, H., Bell, B., Berrisford, P., Hirahara, S., Horányi, A., Muñoz-Sabater, J., Nicolas, J., Peubey, C., Radu, R., Schepers, D., Simmons, A., Soci, C., Abdalla, S., Abellan, X., Balsamo, G., Bechtold, P., Biavati, G., Bidlot, J., Bonavita, M., De Chiara, G., Dahlgren, P., Dee, D., Diamantakis, M., Dragani, R., Flemming, J., Forbes, R., Fuentes, M., Geer, A., Haimberger, L., Healy, S., Hogan, R. J., Hólm, E., Janisková, M., Keeley, S., Laloyaux, P., Lopez, P., Lupu, C., Radnoti, G., de Rosnay, P., Rozum, I., Vamborg, F., Villaume, S., and Thépaut, J.-N.: The ERA5 global reanalysis, Quarterly Journal of the Royal Meteorological Society, 146, 1999–2049, https://doi.org/10.1002/qj.3803, _eprint: https://onlinelibrary.wiley.com/doi/pdf/10.1002/qj.3803, 2020.

Hofmann, E. E., Hedström, K. S., Moisan, J. R., Haidvogel, D. B., and Mackas, D. L.: Use of simulated drifter tracks to investigate general transport patterns and residence times in the Coastal Transition Zone, Journal of Geophysical Research: Oceans, 96, 15 041–15 052, https://doi.org/10.1029/91JC00832, _eprint: https://onlinelibrary.wiley.com/doi/pdf/10.1029/91JC00832, 1991.

Johnson, G. C., Hosoda, S., Jayne, S. R., Oke, P. R., Riser, S. C., Roemmich, D., Suga, T., Thierry, V., Wijffels, S. E., and Xu, J.: Argo—Two Decades: Global Oceanography, Revolutionized, Annual Review of Marine Science, 14, 379–403, https://doi.org/10.1146/annurev-marine-022521-102008, _eprint: https://doi.org/10.1146/annurev-marine-022521-102008, 2022.

Kundu, P. K.: Ekman Veering Observed near the Ocean Bottom, Journal of Physical Oceanography, 6, 238–242, https://doi.org/10.1175/1520-0485(1976)006<0238:EVONTO>2.0.CO;2, publisher: American Meteorological Society Section: Journal of Physical Oceanography, 1976.

https://doi.org/10.5194/egusphere-2022-1450
Preprint. Discussion started: 23 December 2022

LaCasce, J. H.: Statistics from Lagrangian observations, Progress in Oceanography, 77, 1–29, https://doi.org/10.1016/j.pocean.2008.02.002, 2008.

Liu, Y. and Weisberg, R. H.: Evaluation of trajectory modeling in different dynamic regions using normalized cumulative Lagrangian separation, Journal of Geophysical Research: Oceans, 116, https://doi.org/10.1029/2010JC006837, _eprint: https://onlinelibrary.wiley.com/doi/pdf/10.1029/2010JC006837, 2011.

Liu, Y., Weisberg, R. H., Vignudelli, S., and Mitchum, G. T.: Evaluation of altimetry-derived surface current products using Lagrangian drifter trajectories in the eastern Gulf of Mexico, Journal of Geophysical Research: Oceans, 119, 2827–2842, https://doi.org/10.1002/2013JC009710, _eprint: https://onlinelibrary.wiley.com/doi/pdf/10.1002/2013JC009710, 2014.

Lumpkin, R. and Centurioni, L.: NOAA Global Drifter Program quality-controlled 6-hour interpolated data from ocean surface drifting buoys., https://doi.org/10.25921/7ntx-z961, type: dataset; Accessed 2022/12/06, 2019.

Lumpkin, R. and Johnson, G. C.: Global ocean surface velocities from drifters: Mean, variance, El Niño–Southern Oscillation response, and seasonal cycle, Journal of Geophysical Research: Oceans, 118, 2992–3006, https://doi.org/10.1002/jgrc.20210, _eprint: https://onlinelibrary.wiley.com/doi/pdf/10.1002/jgrc.20210, 2013.

Mulet, S., Rio, M.-H., Etienne, H., Artana, C., Cancet, M., Dibarboure, G., Feng, H., Husson, R., Picot, N., Provost, C., and Strub, P. T.: The new CNES-CLS18 global mean dynamic topography, Ocean Science, 17, 789–808, https://doi.org/10.5194/os-17-789-2021, publisher: Copernicus GmbH, 2021.

Poulain, P.-M., Gerin, R., Mauri, E., and Pennel, R.: Wind Effects on Drogued and Undrogued Drifters in the Eastern Mediterranean, Journal of Atmospheric and Oceanic Technology, 26, 1144–1156, https://doi.org/10.1175/2008JTECHO618.1, publisher: American Meteorological Society Section: Journal of Atmospheric and Oceanic Technology, 2009.

Pujol, M.-I., Faugère, Y., Taburet, G., Dupuy, S., Pelloquin, C., Ablain, M., and Picot, N.: DUACS DT2014: the new multi-mission altimeter data set reprocessed over 20 years, Ocean Science, 12, 1067–1090, https://doi.org/10.5194/os-12-1067-2016, publisher: Copernicus GmbH, 2016.

Rio, M.-H.: Use of Altimeter and Wind Data to Detect the Anomalous Loss of SVP-Type Drifter's Drogue, Journal of Atmospheric and Oceanic Technology, 29, 1663–1674, https://doi.org/10.1175/JTECH-D-12-00008.1, publisher: American Meteorological Society Section: Journal of Atmospheric and Oceanic Technology, 2012.

Rio, M.-H. and Hernandez, F.: High-frequency response of wind-driven currents measured by drifting buoys and altimetry over the world ocean, Journal of Geophysical Research: Oceans, 108, https://doi.org/10.1029/2002JC001655, _eprint: https://onlinelibrary.wiley.com/doi/pdf/10.1029/2002JC001655, 2003.

Rio, M. H. and Santoleri, R.: Improved global surface currents from the merging of altimetry and Sea Surface Temperature data, Remote Sensing of Environment, 216, 770–785, https://doi.org/10.1016/j.rse.2018.06.003, 2018.

Rio, M. H., Guinehut, S., and Larnicol, G.: New CNES-CLS09 global mean dynamic topography computed from the combination of GRACE data, altimetry, and in situ measurements, Journal of Geophysical Research: Oceans, 116, https://doi.org/10.1029/2010JC006505, _eprint: https://onlinelibrary.wiley.com/doi/pdf/10.1029/2010JC006505, 2011.

Rio, M.-H., Mulet, S., and Picot, N.: Beyond GOCE for the ocean circulation estimate: Synergetic use of altimetry, gravimetry, and in situ data provides new insight into geostrophic and Ekman currents, Geophysical Research Letters, 41, 8918–8925, https://doi.org/10.1002/2014GL061773, _eprint: https://onlinelibrary.wiley.com/doi/pdf/10.1002/2014GL061773, 2014.

https://doi.org/10.5194/egusphere-2022-1450
Preprint. Discussion started: 23 December 2022

Révelard, A., Reyes, E., Mourre, B., Hernández-Carrasco, I., Rubio, A., Lorente, P., Fernández, C. D. L., Mader, J., Álvarez Fanjul, E., and Tintoré, J.: Sensitivity of Skill Score Metric to Validate Lagrangian Simulations in Coastal Areas: Recommendations for Search and Rescue Applications, Frontiers in Marine Science, 8, https://www.frontiersin.org/articles/10.3389/fmars.2021.630388, 2021.

Sakov, P., Counillon, F., Bertino, L., Lisæter, K. A., Oke, P. R., and Korablev, A.: TOPAZ4: an ocean-sea ice data assimilation system for the North Atlantic and Arctic, Ocean Science, 8, 633–656, https://doi.org/10.5194/os-8-633-2012, publisher: Copernicus GmbH, 2012.

Serra, M., Sathe, P., Rypina, I., Kirincich, A., Ross, S. D., Lermusiaux, P., Allen, A., Peacock, T., and Haller, G.: Search and rescue at sea aided by hidden flow structures, Nature Communications, 11, 2525, https://doi.org/10.1038/s41467-020-16281-x, number: 1 Publisher: Nature Publishing Group, 2020.

Taylor, K. E.: Summarizing multiple aspects of model performance in a single diagram, Journal of Geophysical Research: Atmospheres, 106, 7183–7192, https://doi.org/10.1029/2000JD900719, _eprint: https://onlinelibrary.wiley.com/doi/pdf/10.1029/2000JD900719, 2001.

van Sebille, E., Griffies, S. M., Abernathey, R., Adams, T. P., Berloff, P., Biastoch, A., Blanke, B., Chassignet, E. P., Cheng, Y., Cotter, C. J., Deleersnijder, E., Döös, K., Drake, H. F., Drijfhout, S., Gary, S. F., Heemink, A. W., Kjellsson, J., Koszalka, I. M., Lange, M., Lique, C., MacGilchrist, G. A., Marsh, R., Mayorga Adame, C. G., McAdam, R., Nencioli, F., Paris, C. B., Piggott, M. D., Polton, J. A., Rühs, S., Shah, S. H. A. M., Thomas, M. D., Wang, J., Wolfram, P. J., Zanna, L., and Zika, J. D.: Lagrangian ocean analysis: Fundamentals and practices, Ocean Modelling, 121, 49–75, https://doi.org/10.1016/j.ocemod.2017.11.008, 2018.